American Mineralogist, Volume 96, pages 53–59, 2011

An assessment of the potential benefits of ion implants as trace-element reference material for electron probe X-ray microanalysis: The case of invisible gold

YVES THIBAULT* AND ALLEN R. PRATT

CANMET-MMSL, Natural Resources Canada, 555 Booth Street, Ottawa, Ontario K1A 0G1, Canada

ABSTRACT

The reliability of trace element concentrations obtained by EPMA can be significantly improved with the use of high-quality secondary standards. In the case of Au residing in sulfides, such standards are lacking. Natural materials have heterogeneous Au distribution, whereas synthesis is very difficult. The benefits of using ion implants as trace-element reference material for EPMA were assessed by characterizing grains of magnetite, pyrite and galena implanted with 1×10^{14} to 5×10^{14} Au atoms/cm^2 at energies from 1 to 3 MeV. The first interesting observation is the excellent lateral micrometer-scale homogeneity of the Au levels across the implants. The ratio of analytical to statistical standard deviations never exceeds 1.7. Additionally, the Au X-ray intensities measured by EPMA show excellent correlation with those predicted for multilayered structures used to model the continuous Au concentration profile for the three implants investigated. Small discrepancies arise only at low accelerating voltage. In these situations, the predicted Au X-ray intensities become sensitive to uncertainties in the determination of the location of the Au concentration profile because of insufficient excitation of the bottom of the Au layer. Fortunately, by varying the implantation energy, optimal implants yielding X-ray intensities that are insensitive to uncertainties on the Au depth profile can be obtained for a wide range of accelerating voltages. These results suggest that ion implants may represent excellent EPMA reference material, especially in cases where natural and synthetic standards are unavailable. Interesting materials presenting specific analytical challenges can be engineered due to the excellent control of the implantation parameters.

Keywords: EPMA, ion implants, standards, trace element, Au

INTRODUCTION

To optimize gold ore processing strategies, it is critical to evaluate the levels and distribution of refractory "invisible" Au that can reside either as discrete nanometer-sized inclusions or in solution within common sulfides or their oxidation products (e.g., Cabri et al. 1989; Pratt and Duke 2003; Chouinard et al. 2005; Paktunc et al. 2006; Reich et al. 2006). In conjunction with other analytical techniques such as secondary ion mass spectrometry (SIMS) and laser ablation inductively coupled plasma mass spectrometry (LA-ICPMS), the electron probe X-ray microanalyzer (EPMA) remains an instrument of choice to quantitatively correlate trace concentrations of economically important elements such as Au with chemical and morphological features within a sulfide or oxide grain at optimal spatial resolution. This becomes more relevant with the current performance of wavelength-dispersive diffracting crystals that allows detection limits of a few parts per million and the recent introduction of commercial field-emission EPMA capable of sub-micrometer resolution at low accelerating voltage.

A major obstacle in evaluating the consistency and reliability of trace Au concentrations obtained by EPMA is the lack of high-quality secondary standards that are essential to test the ability to correctly extract peak intensity from the background at minimal theoretical detection limits. Natural sulfides are known to have very heterogeneous distribution of Au and consequently are poor candidates. Moreover, because gold has restricted solubility in most common sulfides and the substitution mechanisms are poorly understood, synthesis routes to produce homogeneous grains with optimal Au concentrations are very limited. In this context, ion implants, typically used as standards for SIMS analyses, were evaluated as trace-element reference material for EPMA. During implantation, the distribution and the total concentration of the ion in a target can be independently and precisely controlled by choosing specific energy and dose respectively. However, the narrow depth distribution of the implanted ions relative to typical electron interaction volumes confers to these materials interesting properties. For example, if treated as a simple bulk homogeneous material when analyzed by EPMA, the X-ray intensities obtained for a specific implant would yield "apparent" Au concentrations that vary as a function of accelerating voltage (Fig. 1). Consequently, the material needs to be considered as a multilayered structure and, as such, requires appropriate correction procedures (e.g., Pouchou and Pichoir 1991; Pouchou 2002).

ANALYTICAL AND CALCULATION METHODS

Au implantation procedure

Centimeter-sized polished massive grains of Au-free (<1 ppm) magnetite, pyrite and galena were implanted with Au ions using a 1.7 MV Tandetron accelerator at the Interface Science Western research center. For magnetite, the dose was 5.0

* E-mail: Yves.Thibault@NRCan.gc.ca

$\times 10^{14}$ Au atoms/cm^2 implanted at an energy of 3 MeV. In the case of pyrite and galena, implantation was done at 1 MeV with a dose of 1.0×10^{14} Au atoms/cm^2. In all cases, the ion beam was normal to the target surface.

Monte Carlo simulation of the Au concentration profile

The Au distribution profile obtained for each implant was simulated using the transport of ions in matter (TRIM) utility from the SRIM software package [version SRIM-2008.4; Ziegler et al. (2008)]. Data input includes the nature of the ion, the implantation energy, the angle of incidence of the ion beam relative to normal and finally the composition and density of the target. The resulting ion distribution is given as normalized concentration per unit dose [(atoms/cm^3)/(atoms/cm^2)] as a function of depth.

Measurement of the Au concentration profile by dynamic SIMS

The concentration depth profile of Au was also measured using a CAMECA IMS 3f dynamic secondary ion mass spectrometer (SIMS) housed at the Surface Science Western facility. The primary ion source was a beam of Cs^+, accelerated to 10 keV and rastered over a 250×250 µm^2 area at the sample with a current of 15 nA. Secondary ion intensities for $^{197}Au^-$, $^{56}Fe^-$, $^{208}Pb^-$, and $^{34}S^-$ were collected with a –180 V offset to suppress molecular interferences. The depth of the resulting crater was measured with a Dektak Profilometer. The sputtering rate was assumed to be constant through the analysis yielding a linear correlation between time and depth.

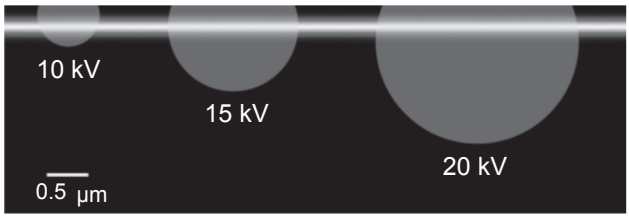

Figure 1. Schematic cross-section of pyrite implanted with Au at 2.0 MeV showing Au distribution in relation with the envelope of electron range at various accelerating voltages [calculated with NISTMonte; Ritchie (2005)]. Au concentration is depicted with a grayscale, white representing the highest level.

Measurement of Au*Mα* and *Lα* X-ray intensities by EPMA

The Au*Mα* and *Lα* X-ray intensities were collected on the implants using a JEOL JXA 8900 EPMA operated at accelerating voltages ranging from 10 to 30 kV, a probe current up to 400 nA, and a beam defocused at 10 µm. To improve counting statistics, three wavelength-dispersive spectrometers (WDS), were used simultaneously, one being equipped with a large H-type diffracting crystal. For each analytical location, three consecutive series of peak and background measurements of 300 s duration were typically made. At each analytical condition, 15 to 20 analyses were done across the centimeter-sized implanted magnetite, pyrite, and galena grains. Background positions were evaluated on Au-free magnetite, pyrite and galena standards. Care was taken to account for a negative anomaly in the background slope near the Au*Lα* position associated with a multiple-diffraction artifact of the LIF crystal (e.g., Self et al. 1990; Robinson and Graham 1992). Intensity ratios (k ratios) were obtained relative to pure Au, which acts as the primary standard.

Calculation of predicted Au X-ray k ratios

For computation of the predicted Au*Mα* and Au*Lα* X-ray k ratios that should be obtained when analyzed by EPMA, the continuous Au depth distribution was simulated using simplified layered structures, where each layer has a fixed Au concentration. Then, the matrix calculations were performed with the GMRfilm software (e.g., Waldo et al. 1993 and references therein) using the Pouchou and Pichoir (1990) $\phi(\rho z)$ model, and incorporating a continuum X-ray fluorescence correction. Data input includes the accelerating voltage, the characteristic X-ray lines, the standards, as well as the known mass depth (ρz) and weight fractions of the elements for all layers. The output yields the contribution of each layer to the k ratios for all elements.

Because of the narrow depth distribution of Au relative to typical electron interaction volume, the simulated profile used for the calculation can be kept quite simple. For example, in Figure 2, a typical Au distribution profile, obtained for pyrite implanted at 2 MeV, and three different layered structures are shown. In the simplest case (Fig. 2a), the total Au is concentrated in one layer, the upper and lower part of which are fixed at positions where the concentrations represent 25% of the maximum in the continuous profile. Two other simplified structures where the Au is distributed in three layers are also shown in Figure 2. In one case (Fig. 2b) the upper and lower boundaries of the central layer are located at positions where the concentration represents 90% of the maximum. The number of Au atoms per unit area (atoms/cm^2) in this layer is calculated by summing the total number of atoms per unit area in the continuous profile contained within this width. The top of the overlying layer and the bottom of the underlying one are located at positions representing 15% of the concentration maximum. The number

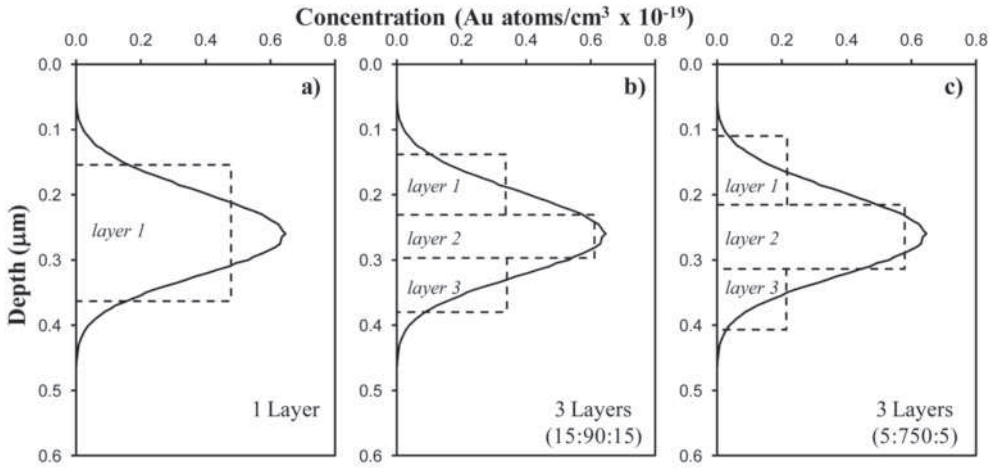

Figure 2. Three simplified layered structures (dashed lines) simulating the continuous concentration profile (solid black line) for pyrite implanted with 1×10^{14} atoms/cm^2 at 2 MeV as calculated by TRIM: (**a**) one-layered structure with boundaries fixed at 25% of the maximum in the continuous profile; (**b**) three-layered structure with boundaries of the central Au layer fixed at 90% of the maximum continuous profile and limits of the top and bottom layers at located at 15% of the concentration maximum; (**b**) three-layered structure with boundaries of the central Au layer fixed at 75% of the maximum continuous profile and limits of the top and bottom layers at located at 5% of the concentration maximum. The predicted k ratios obtained for each scenario are shown in Table 1. See also details in text.

of atoms per unit area in these layers is obtained by summing the total number of atoms per unit area in the continuous profile on each side of the central layer. The other triple-layered structure (Fig. 2c) is constructed with the same logic, but with the boundaries of the central layer located at positions representing 75% of the concentration maximum, and the edges of the upper and lower layers located at 5% of the maximum. In all cases, the bottom substrate and the uppermost region ranging from the surface to the top of the first Au layer are treated as pure matrix (e.g., Fe_3O_4, FeS_2, PbS) free of Au.

To obtain the weight fractions of Au and matrix elements within each layer, the number of Au atoms per unit area is first converted to weight (g/cm^2), knowing the molar weight of Au (196.67 g/mol). The weight per unit area of the matrix (g/cm^2) is also calculated by multiplying its known density (e.g., 5.02 g/cm^3 for FeS_2) by the thickness of the layer (cm). Although an approximation of the Au contribution to the thickness was made by using its density as a pure phase (19.3 g/cm^2), it can actually be ignored due to its low concentration. Finally the weight fractions of Au and matrix within each layer are obtained as the ratio of their specific weight by the total weight.

As can be seen in Table 1, although the contribution of each layer changes, the predicted total k ratios obtained for the three very distinct scenarios, described above, are similar within better than 1% relative. This suggests that these simplified layered structures are, indeed, adequate to simulate the continuous concentration profile.

Results and discussion

Magnetite implanted with 5×10^{14} Au atoms/cm^2 at 3 MeV

The concentration profiles simulated by SRIM and measured by SIMS for the magnetite implanted with 5×10^{14} Au atoms/cm^2 at an energy of 3 MeV can be found in Figure 3. The SIMS-measured Au ion distribution has a wider spread, tailing slightly deeper than the one predicted by the TRIM simulation. This difference in spread, estimated by comparing the full-width at half maximum (FWHM) for the two distributions, is in the order of 5% relative. Evidently, both profiles have the same area under the curve reflecting the total amount of implanted Au ions (5×10^{14} Au atoms/cm^2).

The variations in the predicted Au$M\alpha$ and Au$L\alpha$ k ratios as a function of accelerating voltage for both profiles are shown in Figure 4. With decreasing accelerating voltage, there is initially a continuous increase in the k ratios, related to an increase in the relative proportion of Au in a decreasing excitation volume (e.g., Fig. 1). This is followed by a sharp drop reflecting that, at lower voltage, the depth of Au$M\alpha$ X-ray production range does not reach the bottom of the implanted Au layer anymore. As discussed above, the bottom of the SIMS-measured profile is deeper than the TRIM-simulated one and this explains why the

Table 1. Comparison of predicted k ratios for three layered structures used to simulate the continuous Au concentration profile obtained with 1×10^{14} Au atoms/cm^2 implanted in pyrite at 2 MeV (see also Fig. 2)

Layered structure type*	Accelerating voltage (kV)	X-ray line	k ratio Layer 1	Layer 2	Layer 3	Total
1 Layer	10	Au*M*α				0.884
	15					0.865
	25	Au*L*α				0.384
	30					0.270
3 Layers (15:90:15)	10	Au*M*α	0.394	0.335	0.151	0.880
	15		0.294	0.353	0.214	0.861
	25	Au*L*α	0.122	0.156	0.106	0.384
	30		0.082	0.109	0.078	0.269
3 Layers (5:75:5)	10	Au*M*α	0.317	0.476	0.092	0.886
	15		0.215	0.500	0.142	0.857
	25	Au*L*α	0.088	0.222	0.074	0.384
	30		0.059	0.155	0.055	0.270

* See Figure 1 and text for more details on the layered structure profiles.

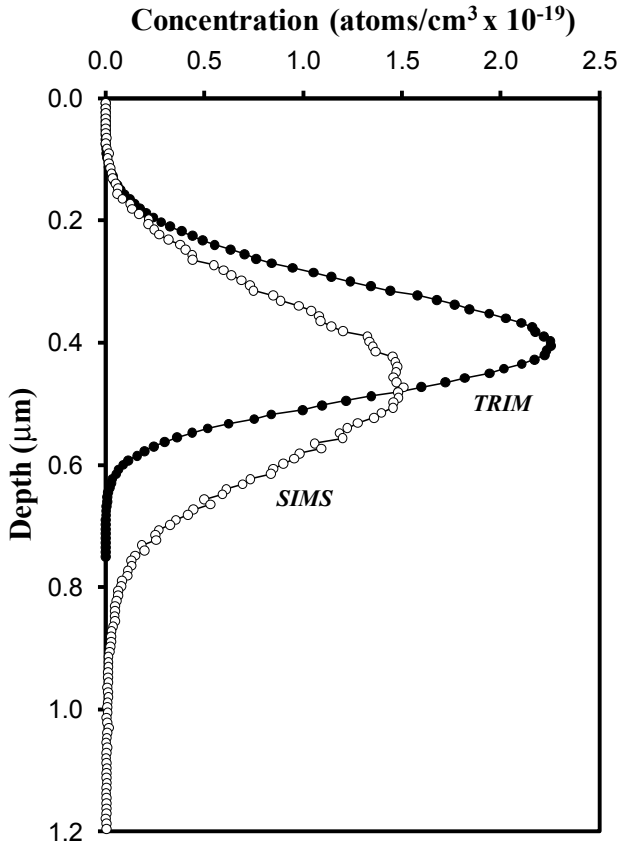

Figure 3. TRIM-simulated (filled circles) and SIMS-measured (empty circles) Au concentration profiles for magnetite implanted with 5×10^{14} Au atoms/cm^2 at an energy of 3 MeV. The area under the curve, representing the total number of Au atoms per area, is the same for both profiles.

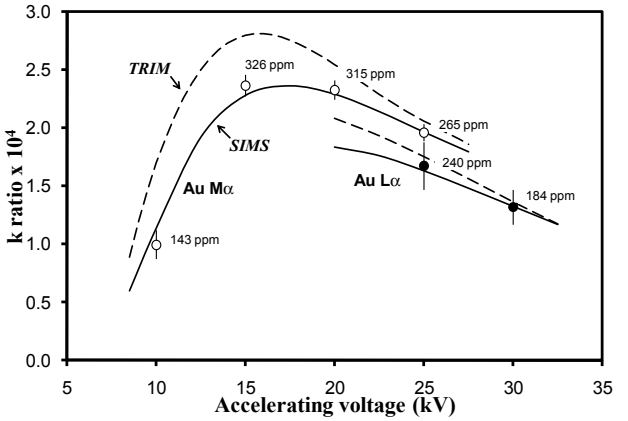

Figure 4. Au$M\alpha$ and Au$L\alpha$ k ratios as a function of accelerating voltage for magnetite implanted with 5×10^{14} Au atoms/cm^2 at 3 MeV. Solid lines and dashed lines depict the predicted k ratios calculated for the SIMS-measured and TRIM-simulated Au profiles, respectively. The average Au$M\alpha$ and Au$L\alpha$ k ratios measured by EPMA are shown as empty and filled circles respectively. Error bars represent 2× the standard deviation based on counting statistics for each individual analysis. Average EPMA measurements are labeled with the concentrations obtained from the k ratio assuming a homogeneous distribution of Au with depth within the excitation volume.

Table 2. EPMA results obtained for magnetite, pyrite, and galena implants

Accelerating voltage (kV)	k ratio × 10^4 (avg.)	N	σ_a	σ_s	σ-ratio (σ_a/σ_s)	Apparent concentration (ppm)
Magnetite; 5 × 10^{14} Au atoms/cm² at 3.0 MeV						
	Au*M*α					
10	0.994	20	6.66	6.25	1.07	143
15	2.366	20	1.93	1.97	0.98	326
20	2.327	20	1.52	1.77	0.86	315
25	1.960	20	2.24	1.92	1.17	265
	Au*L*α					
25	1.673	15	7.71	6.12	1.25	240
30	1.319	20	9.70	5.70	1.70	184
Pyrite; 1 × 10^{14} Au atoms/cm² at 1.0 MeV						
	AuMα					
10	1.585	20	3.10	4.95	0.63	216
15	1.021	20	4.43	4.88	0.91	128
20	0.692	20	5.37	6.22	0.86	81
25	0.510	20	7.13	8.37	0.85	57
Galena; 1 × 10^{14} Au atoms/cm² at 1.0 MeV						
	Au*M*α					
10	1.251	20	8.31	8.75	0.95	131
15	1.043	20	6.05	6.56	0.92	109
20	0.775	20	6.72	7.72	0.87	80
25	0.642	20	9.29	8.85	1.05	66

Notes: N = number of analyses; σ_a = analytical standard deviation expressed as percent relative; σ_s = standard deviation based on counting statistics expressed as percent relative for each individual analysis. Apparent concentrations are calculated from the k ratios assuming a homogenous distribution of Au within depth throughout the specimen.

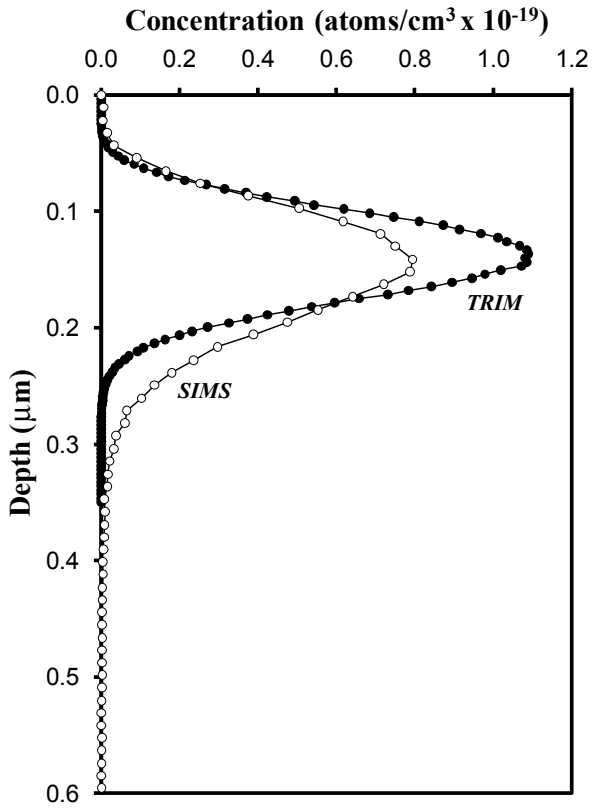

Figure 5. TRIM-simulated (filled circles) and SIMS-measured (empty circles) Au concentration profiles for pyrite implanted with 1 × 10^{14} Au atoms/cm² at an energy of 1 MeV. The area under the curve, representing the total number of Au atoms per area, is the same for both profiles.

sharp drop in X-ray intensity occurs at slightly higher voltage (17.5 vs. 16 kV). Moreover, the wider spread of the SIMS profile (Fig. 3) results in a lower proportion of Au ions concentrated at the optimal X-ray generation depth of the excitation volume explaining the lower k ratio at a given voltage. This effect becomes minimal at higher accelerating voltages because the Au depth distribution becomes very narrow in comparison to the larger excitation volume.

The measured Au*M*α and Au*L*α k ratios obtained by EPMA at various accelerating voltages on the magnetite implant are listed in Table 2 and plotted in Figure 4. Within uncertainties, the measured k ratios at each accelerating voltage condition are in very good agreement with the predicted ones for the SIMS-measured profile. It is practical to evaluate what these X-ray intensities would relate to, in terms of concentration, in an unknown where the Au is distributed homogeneously with depth. Such concentration is referred to as "apparent" because the Au concentration in the implant, although very precisely controlled, is not homogenous with depth. The apparent bulk Au concentrations that would be obtained from these measured k ratios range from 143 to 326 ppm.

The level of lateral micrometer-scale homogeneity in the Au level across the centimeter-sized grain of magnetite is excellent. The degree of homogeneity was estimated by calculating a σ-ratio defined as the ratio of the analytical standard deviation obtained for 15 to 20 analyses at each analytical condition to the statistical standard deviation based on counting statistics (cf. Carpenter et al. 2002). Low σ-ratios of 0.86 to 1.7 were obtained with theoretical relative standard errors ranging from 1.5 to 6.25% (Table 2).

Pyrite implanted with 1 × 10^{14} Au atoms/cm² at 1 MeV

The Au implantation for pyrite was done at significantly lower energy (1 MeV) than for magnetite (3 MeV). Consequently, as illustrated in Figure 5, the TRIM-simulated and SIMS-measured Au distributions are narrower with concentration maxima at much shallower depth (≈0.14 μm). Once again, the SIMS-measured profile tails off slightly deeper than the TRIM-simulated one. The relative difference in the distribution spread between the two profiles calculated at FWHM is 4%, fairly close to the one observed for magnetite (5%).

The predicted Au*M*α k ratios for both concentration profiles progressively increase with decreasing accelerating voltage. Additionally, because the depth of X-ray production range is always below the bottom of the relatively shallow layer of Au, no sharp drop in Au*M*α X-ray intensity, as was observed in the case of magnetite, is predicted at accelerating voltages down to at least 10 kV. The similarity in the evolution of the predicted k ratio as a function of accelerating voltage between SIMS-measured and TRIM-simulated profiles can be explained by the fact that, in both cases, Au is concentrated at shallow depth in a narrow region well within the optimal X-ray generation depth of the excitation volume for a wide range of accelerating voltages.

The Au*M*α X-ray intensities obtained by EPMA (Table 2; Fig. 6) are in good agreement with the predicted ones, although they appear significantly higher at 10 kV (Fig. 5). The apparent bulk concentrations calculated for the measured k ratios ranged from 216 ppm at 10 kV to 57 ppm at 25 kV (Table 2). These

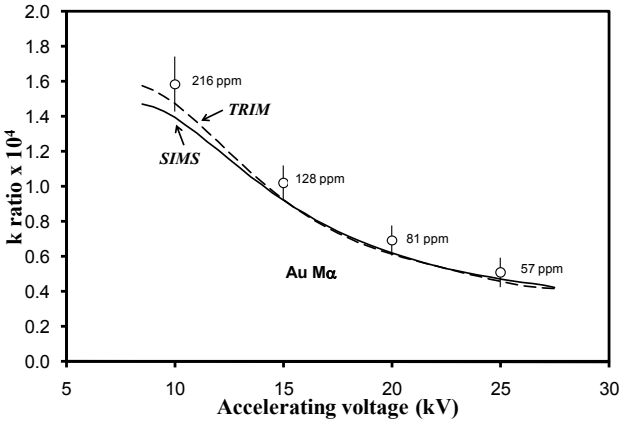

FIGURE 6. Au$M\alpha$ k ratios as a function of accelerating voltage for pyrite implanted with 1×10^{14} Au atoms at 1 MeV. Solid lines and dashed lines depict the predicted k ratios calculated for the SIMS-measured and TRIM-simulated Au profiles, respectively. The average Au$M\alpha$ k ratios measured by EPMA are shown as empty circles. Error bars represent 2× the standard deviation based on counting statistics for each individual analysis. Average EPMA measurements are labeled with the concentration obtained from the k ratio assuming a homogeneous distribution of Au with depth within the excitation volume.

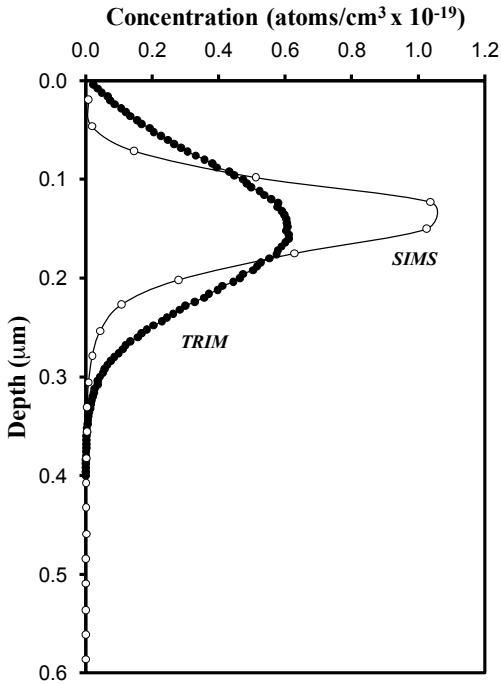

FIGURE 7. TRIM-simulated (filled circles) and SIMS-measured (empty circles) Au concentration profiles for galena implanted with 1×10^{14} Au atoms/cm^2 at an energy of 1 MeV. The area under the curve, representing the total number of Au atoms per area, is the same for both profiles.

significantly lower values compared to magnetite are evidently related to the lower implantation dose of 1×10^{14} atoms/cm^2 used for pyrite as opposed to 5×10^{14} Au atoms/cm^2 for magnetite. Homogeneity is excellent, as indicated by σ-ratios ranging from 0.63 to 0.91 at theoretical relative standard errors ranging from 4.88 to 8.37% (Table 2).

Galena implanted with 1×10^{14} Au atoms/cm^2 at 1 MeV

Galena was implanted with the same dose and energy conditions used for pyrite. Therefore, this represents a good comparison with a phase having a higher density and mean atomic number. In this case, the TRIM-simulated profile is wider than the SIMS-measured one, but the depth of the concentration maxima is very close at about 0.14 μm (Fig. 7).

As was the case for pyrite, there is a steady increase in predicted k ratios with decreasing accelerating voltages down to 10 kV (Fig. 8). Moreover, there is essentially no divergence observed in the prediction of the Au intensity between the TRIM-simulated and SIMS-measured Au concentration profiles.

The agreement between the Au$M\alpha$ k ratios measured by EPMA (Table 2; Fig. 8) and the predicted ones is excellent at all accelerating voltages investigated (10–25 kV). Those would correspond to apparent bulk Au concentration of 131 ppm at 10 kV to 66 ppm at 25 kV (Table 2; Fig. 7). The high level of homogeneity that can be obtained with implantation is once again demonstrated with σ-ratios ranging from 0.87 to 1.05 at theoretical relative standard errors of 6.56 to 8.85% (Table 2).

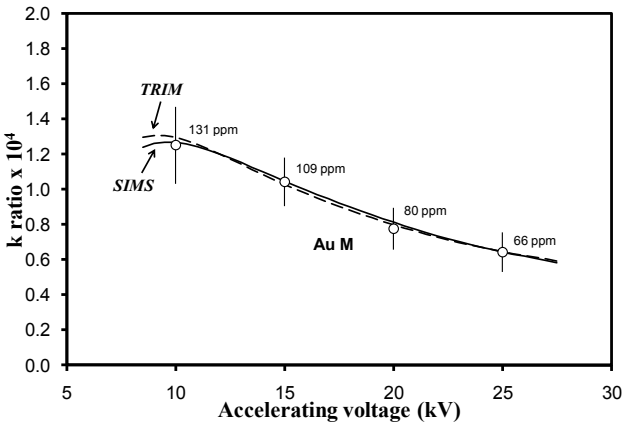

FIGURE 8. Au$M\alpha$ k ratios as a function of accelerating voltage for galena implanted with 1×10^{14} Au atoms/cm^2 at 1 MeV. Solid lines and dashed lines depict the predicted k ratios calculated for the SIMS-measured and TRIM-simulated Au profiles respectively. The average Au$M\alpha$ k ratios measured by EPMA are shown as empty circles. Error bars represent 2× the standard deviation based on counting statistics for each individual analysis. Average EPMA measurements are labeled with the concentration obtained from the k ratio assuming a homogeneous distribution of Au with depth within the excitation volume.

Optimization of implantation parameters

In all cases investigated, the agreement between the measured k ratios and those predicted with the SIMS-measured Au concentration profiles are quite good. Considering also the excellent level of homogeneity, we propose that such ion implants may represent interesting reference materials that would be very useful in evaluating our ability to measure Au X-ray intensities at minimal detection limits.

Ideally, the knowledge of the Au depth distribution for a given implant will be highly accurate. In this context, the very good agreement, for all the implants investigated, between the Au X-ray intensities measured by EPMA and those predicted

from the concentration profiles determined by SIMS demonstrates the expected high reliability of the SIMS measurements compared to the TRIM simulation. However, practically, the ideal implant reference material would be one where the predicted k ratios are the less sensitive to uncertainties in the determination of the shape and location of the Au concentration profile. Preferably, the implant will also be reliable for a wide range of analytical conditions.

In Figure 9a, TRIM-simulated Au concentration profiles calculated for hypothetical pyrite specimens implanted with 1×10^{14} atoms/cm^2 at an energy ranging from 1 to 3 MeV are shown. The predicted Au$M\alpha$ k ratios obtained as a function of accelerating voltage for these simulated Au concentration profiles are then compared in Figure 9b. Interestingly, at high accelerating voltages, no significant differences in the predicted k ratios are observed between the hypothetical implants indicating that large changes in the Au concentration profile have negligible effect on the resulting Au$M\alpha$ X-ray intensities at these analytical conditions. With decreasing accelerating voltages, significant divergence is initiated when X-ray production starts to drop due to insufficient excitation of the lower part of the Au layer. Based on these observations, optimal implantation energy for a given range of analytical conditions can be empirically determined by simply locating the minima in the first derivative of the evolution of k ratios with accelerating voltage (Fig. 9c). As can be seen in Figure 9b, these minima predict very well the position of the divergent points in Au$M\alpha$ X-ray intensities at 21, 17, 14.5, and 13.5 kV for the 3, 2, 1.5, and 1.25 MeV implants, respectively. With this in mind, for a given implantation energy, the X-ray intensities will be quite insensitive to uncertainties on the Au depth profile (e.g., TRIM-simulated vs. SIMS-measured), as long as the accelerating voltage conditions are kept beyond the location of the minimum in the derivative plot (Fig. 9c). Consequently, of all the cases depicted in Figure 9a, the 1 MeV implant represents the best alternative to cover the widest range of accelerating voltage starting from about 12 kV (Fig. 9c), which is consistent with the results obtained on the pyrite implant. At lower accelerating voltage conditions, that may be preferred to further improve spatial resolution with a field-emission EPMA, lower implantation energy can be chosen, although care will need to be taken as the resulting narrow distribution very close to the surface will render the implant more susceptible to minor surface modification.

Once an appropriate implantation energy is established, an optimal implantation dose can be chosen. For example, the Au X-ray intensities obtained for the three implants used in this study

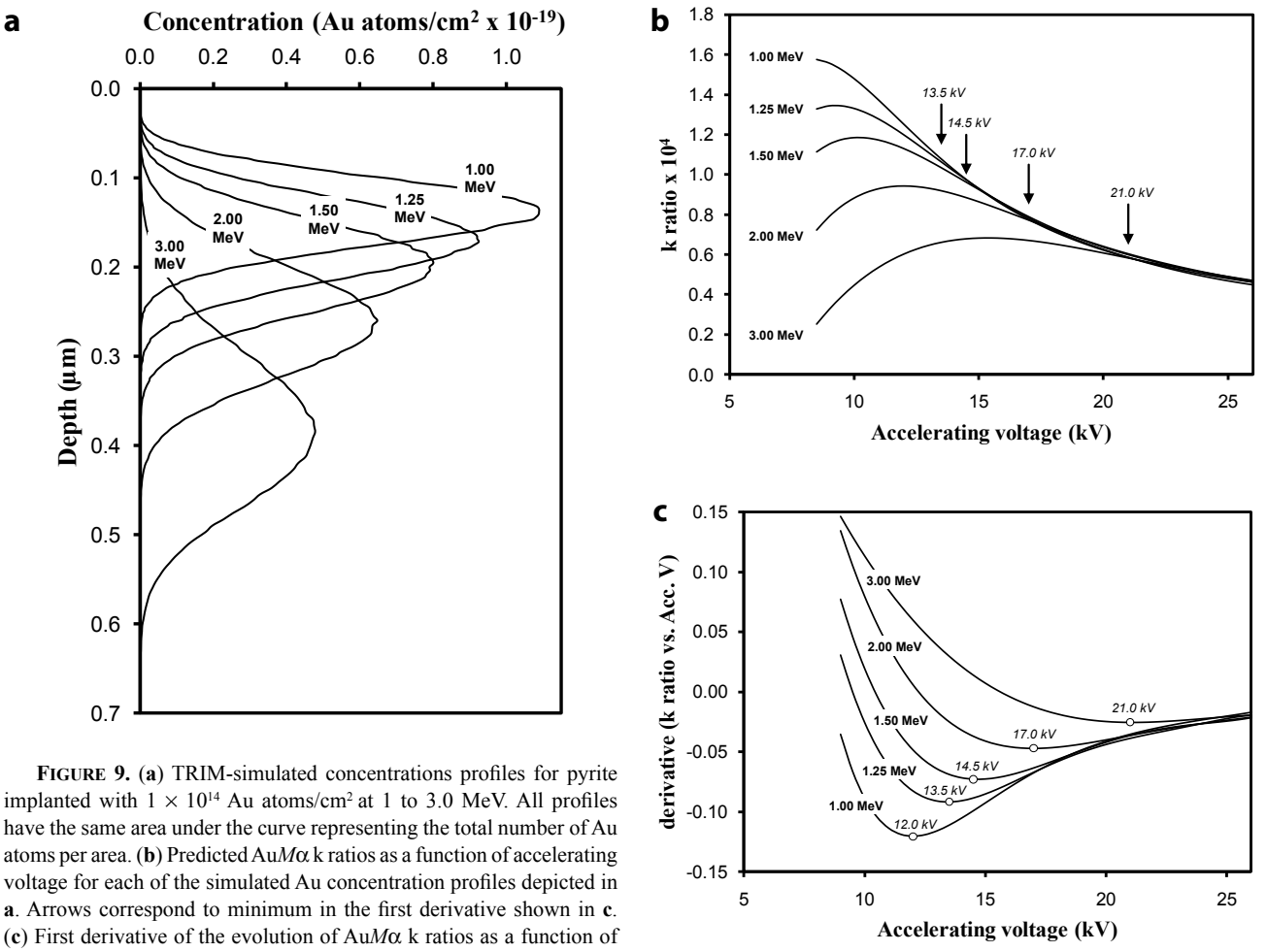

Figure 9. (**a**) TRIM-simulated concentrations profiles for pyrite implanted with 1×10^{14} Au atoms/cm^2 at 1 to 3.0 MeV. All profiles have the same area under the curve representing the total number of Au atoms per area. (**b**) Predicted Au$M\alpha$ k ratios as a function of accelerating voltage for each of the simulated Au concentration profiles depicted in **a**. Arrows correspond to minimum in the first derivative shown in **c**. (**c**) First derivative of the evolution of Au$M\alpha$ k ratios as a function of accelerating voltage. The empty circles represent the minima and are labeled with the corresponding accelerating voltages.

yield "apparent" bulk concentrations ranging from 57 to 320 ppm for the analytical conditions investigated. However, X-ray intensities corresponding to lower Au abundances can easily be tested, by using lower implantation dose.

Based on these considerations, the pyrite and galena implants that were investigated are considered optimal for use at accelerating voltages down to 12 kV. This is emphasized by the fact that, for both pyrite and galena, the predicted Au X-ray intensities as a function of accelerating voltages (Figs. 6 and 8) are fairly insensitive to the observed difference in the TRIM-simulated and SIMS-measured concentration profiles (Figs. 5 and 7). These implants would be ideal to evaluate X-ray intensities corresponding to Au concentrations as low as 60 ppm. However, to investigate the ability to reach detection limits down to 10 ppm, pyrite and galena grains could easily be implanted at the same energy, but with a lower dose (e.g., 2.0×10^{13} Au atoms/cm^2).

On the other hand, although the magnetite implant is a nice example of the evolution of X-ray intensities as a function of accelerating voltages in layered structures, it is not considered ideal as a trace-element reference material. The energy used during implantation was too high with Au being concentrated too deep in the magnetite matrix. Consequently, the lower part of the Au layer cannot be reached in the lower range of accelerating voltages resulting in a sharp drop in Au$M\alpha$ X-ray production and significant divergence in X-ray intensities predicted from the SIMS-measured and TRIM-simulated concentration profiles. Fortunately, an optimal magnetite implant could easily be made by using a lower implantation energy (e.g., 1 MeV).

Applications

There are two major aspects of EPMA that have a direct impact on the quality of the analyses performed. The first involves the precise measurement of the characteristic X-ray intensities on an unknown relative to a primary standard (k ratio), whereas the second consists in performing a proper matrix correction to transform the measured X-ray intensities into mass fraction of the element of interest. In major element analyses, X-ray spectral measurement is typically straightforward, however, the choice of a homogeneous primary standard of composition close to the unknown and the quality of the matrix correction are key to obtain an accuracy as close as possible to the high analytical precision obtained (e.g., Armstrong 2009). The challenges are significantly different when dealing with trace elements. In this case, although the choice of a reliable primary standard remains very important, the proper extraction of the low characteristic X-ray intensity from the background clearly becomes the most critical factor in obtaining the correct element concentration within analytical precision based on counting statistics. Moreover, with the improved collection efficiency of modern wavelength-dispersive diffracting crystals, progressively lower theoretical detection limits can be reached. At such low levels, minor artifacts in the shape of the background, such as curvature or holes (e.g., Self et al. 1990), that are not properly accounted for, can lead to major errors. Consequently, we believe that it is becoming imperative to rely on highly homogeneous trace-element reference material to precisely evaluate our ability to correctly measure the characteristic X-ray intensities in a specific matrix (e.g., magnetite, pyrite, galena, etc.) as the detection levels are approached. The results of this study strongly suggest that ion implants may represent unique candidates to fulfill this role. They have a remarkable level of micrometer-scale homogeneity and, due to the excellent control of the implantation parameters, they can be precisely engineered to yield very low, yet highly predictable and reproducible characteristic X-ray intensities for a variety of trace elements in many types of matrices, especially in cases, such as gold, where conventional synthesis is difficult. The possibility of implanting large areas homogeneously would also allow distribution to different facilities for inter-laboratory comparison. Evidently, because of the narrow element distribution relatively close to the surface, implants need to be handled with care to preserve a relatively pristine surface, as subsequent re-polishing is not possible.

Acknowledgments

We thank W. Lennard and J. Hendriks from the Interface Science Western research center for the implantation work as well as S. Dimov and G. Good for performing the SIMS analyses at Surface Science Western. Rolando Lastra provided helpful suggestions throughout the course of this investigation. Finally, we appreciate the objectives comments from Barry Bickmore, the associate editor, and two anonymous reviewers.

References cited

Armstrong, J.T. (2009) Improving EPMA standards and standards measurement by updating correction parameters, refining measurement procedures, and accounting for surface coatings. EOS, 90, San Francisco Fall Meeting Supplement, Abstract V33E-02.

Cabri, L.J., Chryssoulis, S.L., De Villers, J.P.R., Laflamme, J.H.G., and Buseck, P.R. (1989) The nature of "invisible" gold in arsenopyrite. Canadian Mineralogist, 27, 353–362.

Carpenter, P., Counce, D., Kluk, E., and Nabelek, C. (2002) Characterization of corning EPMA standard glasses 951VR, 951IRW, and 951RX. Journal of Research of the National Institute of Standards and Technology, 107, 703–718.

Chouinard, A., Paquette, J., and Williams-Jones, A. (2005) Crystallographic controls on trace-element incorporation in auriferous from the Pascua epithermal high-sulfidation deposit, Chile-Argentina. Canadian Mineralogist, 43, 951–963.

Paktunc, D., Kingston, D., Pratt, A.R., and McMullen, J. (2006) Distribution of gold in pyrite and in products of its transformation resulting from roasting of refractory gold ore. Canadian Mineralogist, 44, 213–227.

Pouchou, J.L. (2002) X-ray microanalysis of thin surface films and coatings. Microchimica Acta, 138, 133–152.

Pouchou, J.L. and Pichoir, F. (1990) Surface film X-ray microanalysis. Scanning, 12, 212–224.

——— (1991) Quantitative analysis of homogeneous or stratified microvolumes applying the model PAP. In K.F.J. Heinrich and D.E. Newbury, Eds., Electron Probe Quantitation, p. 31–76. Plenum Press, New York.

Pratt, A.R. and Duke, N. (2003) Characterizing the distribution of gold in pyritic sulfide ore. Journal of Minerals, Metals, and Materials, 55, 48–51.

Reich, M., Utsunomiya, S., Kesler, S.E., Wang, L., Ewing, R.C., and Becker, U. (2006) Thermal behavior of metal nanoparticles in geologic materials. Geology, 34, 1033–1036.

Ritchie, N.W.M. (2005) A new Monte Carlo application for complex sample geometries. Surface and Interface Analysis, 37, 1006–1011.

Robinson, B.W. and Graham, J. (1992) Advances in electron microprobe trace-element analysis. Journal of Computer-Assisted Microscopy, 4, 263–265.

Self, P.G., Norrish, K., Milnes, A.R., Graham, J., and Robinson, B.W. (1990) Holes in the background in XRS. X-ray Spectrometry, 19, 59–61.

Waldo, R.A., Militello, M.C., and Gaarenstroom, S.W. (1993) Quantitative Thin-film analysis with an energy-dispersive X-ray detector. Surface and Interface Analysis, 20, 111–114.

Ziegler, J.F., Biersack, J.P., and Ziegler, M.D. (2008) SRIM—The Stopping and Range of Ions in Matter, 398 p. Lulu Press, Morrisville, North Carolina.

Manuscript received December 21, 2009
Manuscript accepted August 19, 2010
Manuscript handled by Barry Bickmore